DR ALI AHMAD NAZ (Orcid ID : 0000-0002-0382-2128)
DR AXEL MITHÖFER (Orcid ID : 0000-0001-5229-6913)
DR TINA KYNDT (Orcid ID : 0000-0002-5267-5013)
DR SHAHID SIDDIQUE (Orcid ID : 0000-0001-7503-4318)

Article type : Regular Manuscript

Title: Plant parasitic cyst nematodes redirect host indole metabolism via NADPH oxidase-mediated ROS to promote infection

Divykriti Chopra[1,*], M. Shamim Hasan[1,2,*,0000-0001-6417-9650], Christiane Matera[1], Oliver Chitambo[1], Badou Mendy[1], Sina-Valerie Mahlitz[1], Ali Naz[3,0000-0002-0382-2128], Shelly Szumski[4], Slawomir Janakowski[5], Miroslaw Sobczak[5,0000-0002-4660-6935], Axel Mithöfer[6,0000-0001-5229-6913], Tina Kyndt[7,0000-0002-5267-5013], Florian M. W. Grundler[1, 0000-0001-8101-0558], Shahid Siddique[1, 4, †,0000-0001-7503-4318]

Affiliations:

[1]Rheinische Friedrich-Wilhelms-University of Bonn, INRES - Molecular Phytomedicine, Karlrobert- Kreiten-Straße 13, D-53115 Bonn, Germany

[2]Department of Plant Pathology, Faculty of Agriculture, Hajee Mohammad Danesh Science and Technology University, Dinajpur 5200, Bangladesh

[3]Department of Plant Breeding, Institute of Crop Science and Resource Conservation, University of Bonn, D-53115 Bonn, Germany

[4]Department of Entomology and Nematology, University of California, Davis, One Shields Ave., Davis, CA 95616, USA

[5]Department of Botany, Warsaw University of Life Sciences (SGGW), Institute of Biology, PL-02-787 Warsaw, Poland

[6]Research Group Plant Defense Physiology, Max Plank Institute for Chemical Ecology, Hans-Knöll-Straße 8, D-07745 Jena, Germany

[7]Department Biotechnology, Research Group Epigenetics & Defence, Coupure links 653, B-9000 Gent, Belgium

*equal contribution

†Correspondence: ssiddique@ucdavis.edu

Received: 3 February 2021

Accepted 11 June 2021

Summary

- Reactive oxygen species (ROS) generated in response to infections often activate immune responses in eukaryotes including plants. In plants, ROS are primarily produced by plasma membrane-bound NADPH oxidases called respiratory burst oxidase homolog (Rboh). Surprisingly, Rbohs can also promote the infection of plants by certain pathogens, including plant parasitic cyst nematodes.
- The Arabidopsis genome contains 10 Rboh genes (*RbohA*–*RbohJ*). Previously, we showed that cyst nematode infection causes a localized ROS burst in roots, mediated primarily by *RbohD* and *RbohF*. We also found that plants deficient in *RbohD* and *RbohF* (*rbohD/F*) exhibit strongly decreased susceptibility to cyst nematodes, suggesting that Rboh-mediated ROS plays a role in promoting infection. However, little is known of the mechanism by which Rbohs promote cyst nematode infection.
- Here, using detailed genetic and biochemical analyses, we identified WALLS ARE THIN1 (WAT1), an auxin transporter, as a downstream target of Rboh-mediated ROS during parasitic infections. We found that WAT1 is required to modulate the host's indole metabolism, including indole-3-acetic acid levels, in infected cells and that this reprogramming is necessary for successful establishment of the parasite.
- In conclusion, this work clarifies a unique mechanism that enables cyst nematodes to use the host's ROS for their own benefit.

Keywords: cyst nematodes, plant parasitic nematodes, root-knot nematodes, ROS promotes parasitic infection, Rboh, syncytium,

Introduction

The oxidative burst, a rapid and transient release of large amounts of reactive oxygen species (ROS), is an essential eukaryotic mechanism for defense against a broad range of microorganisms (Ha *et al*., 2005). In plants, plasma membrane-bound NADPH oxidases, designated as Rbohs (for respiratory burst oxidase homologs), are the main source of ROS during pathogen-induced oxidative bursts (Daudi *et al*., 2012; Torres *et al*., 2002*;* Torres *et al*., 1998). The role of Rboh-produced ROS in activating plant defense has long been known (Torres and Dangl, 2005), but Rbohs also promote the infection of plants by various pathogens (Torres *et al*., 2017; Marino *et al*., 2012; Proels *et al*., 2010; Asai and Yoshioka, 2009; Pogány *et al*., 2009; Trujillo *et al*., 2006; Torres *et al*., 2002). Despite this intriguing contradiction, the mechanisms by which NADPH oxidases promote pathogen infection remain obscure.

Among several types of plant pathogens, plant parasitic nematodes (PPNs) are one of the most destructive and cause huge losses in crop production annually (Nicol *et al*., 2011). Most of the damage caused by PPNs is due to a small group of root-infecting sedentary endoparasitic nematodes that includes cyst nematodes and root-knot nematodes. The cyst and root-knot nematode infection process can be divided into two major stages: 1) root invasion and induction of a feeding site and 2) long-time feeding site maintenance and nutrient acquisition. During the first stage, infective juveniles (termed J2s) invade the plant roots and migrate through different tissue layers to reach the vascular cylinder (Marhavy *et al*., 2019; Holbein *et al*., 2019). Once there, cyst nematodes induce development of a syncytium, whereas root-knot nematodes induce five to seven giant cells, and both types of parasites become sedentary. During the subsequent nutrient acquisition stage, initial feeding sites expand, leading to the formation of hypermetabolic

sinks from which nematodes draw their nutrients. The development of these feeding sites is accompanied by profound structural and physiological changes in host plants (Siddique and Grundler, 2018; Smant *et al*., 2018; Gheysen and Mitchum, 2018; Siddique and Grundler, 2015).

Previously, we showed that cyst nematode infection causes a localized ROS burst in Arabidopsis roots, mediated primarily by RbohD and RbohF complexes, with no observable contribution from the other eight members of the *Rboh* gene family. We also found that plants deficient in RbohD and RbohF (*rbohD/F*) exhibit strongly decreased susceptibility to cyst nematodes, suggesting that Rboh-mediated ROS plays a role in promoting infection (Siddique *et al*., 2014). Here, using comparative transcriptomics and functional analyses, we explored the mechanism by which NADPH oxidases promote plant infection by examining the plant response to cyst nematodes and root-knot nematodes. We identified a vacuolar protein, WALLS ARE THIN1 (WAT1), as a downstream target of Rboh-mediated ROS. We found that WAT1 redirects host indole metabolism, including auxin accumulation, in infected cells, thus promoting infection.

Materials and Methods

Plant material and culture conditions

Seeds of *Arabidopsis thaliana* Columbia-0 (Col-0) and mutant lines *rbohD/F*, *rbohD* (Torres *et al.,* 2002), and *wat1 (*Ranocha *et al*., 2010*)* were surface sterilized by washing in 70% (v/v) ethanol for 5 min followed by washing with 2% (w/v) sodium hypochlorite for 3 min and rinsing twice with sterile water. Seeds were dried on sterile Whatman filter paper or stored at 4°C before plating. Arabidopsis plants were grown at a constant temperature of 23°C, under long-day conditions with 16 h light and 8 h darkness in Petri dishes containing agar medium supplemented with modified Knop nutrient solutions for cyst nematode infection or Murashige and Skoog (MS) medium for root knot infection as described previously (Sijmons *et al*., 1991). Primers used to genotype the mutant lines are available in Table S1.

Nematode infection assays

Heterodera schachtii second-stage juveniles (J2) were harvested from mono-culture as previously described (Shah *et al*., 2017). For the cyst nematode infection assay, 60–80 J2s were sterilized with 0.05% (w/v) $HgCl_2$, extensively washed in sterile water, and inoculated onto the surface of an agar Knop medium plate containing two 12-day-old Arabidopsis plants under sterile conditions. For each experiment, 15–20 plants were used per genotype, and experiments were repeated at least three times independently. The numbers of female nematodes per plant were counted at 12 days post inoculation (dpi). The sizes of the female nematodes and syncytia were measured at 14 dpi using a Leica DM2000 (Leica Microsystems, Germany) dissecting

microscope. The syncytia or female nematodes were outlined, and the area was calculated using LAS software (Leica Microsystems, Germany).

Meloidogyne incognita was propagated on greenhouse cultures of tomato (*Solanum lycopersicum* cv. Moneymaker) plants. As described previously (Mendy *et al*., 2017), galls on roots of tomato were cut into smaller pieces of approximately 1 cm, crushed, and incubated for 3 min in 1.5% (w/v) sodium hypochlorite. Subsequently, the suspension was passed through a series of sieves to separate nematode eggs from root debris, and eggs were collected in a 25-µm mesh sieve. For surface sterilization, eggs were incubated in a 10% (w/v) sodium hypochlorite for 3 minutes and washed abundantly with sterile water. The suspension was stored at RT in darkness. Freshly hatched J2s were rinsed in water and incubated for 20 minutes in 0.5% (w/v) streptomycin-penicillin and 0.1% (w/v) ampicillin-gentamycin solution and for 3 minutes in 0.1% (v/v) chlorhexidine followed by three washes with liberal amounts of sterile autoclaved water. For infection assays with root-knot nematodes, approximately 100 sterile J2s of *M. incognita* were inoculated onto the surface of agar MS-Gelrite medium plates containing two 12-day-old Arabidopsis plants, and the number of galls was counted at 21 dpi. For each experiment, 15–20 plants were used per genotype, and experiments were repeated at least three times independently.

Statistical analyses

For each nematode infection assay, 15–20 plants were used per genotype, and experiments were repeated multiple times and at least three times independently. Data were analyzed for normal distribution (Gaussian) using a Shapiro-Wilk normality test ($\alpha < 0.05$). Normally distributed data were analyzed by either *t*-test (two means; $\alpha < 0.05$) or ANOVA (multiple means; $\alpha < 0.05$) using GraphPad Prism (V: 8.3.0). ANOVA was followed by appropriate posthoc tests (e.g., Tukey's HSD). A non-parametric test, if appropriate, was performed to analyze the data (Kruskal-Wallis test).

Microarray analysis

Ten hours after inoculation with *H. schachtii* J2s, short root segments containing stylet thrusting nematodes were marked under a stereomicroscope. Movements of stylets indicate that J2s are still in the migration phase. The infected area around the nematode head was then dissected and collected in liquid N_2. Care was taken not to collect any tip or lateral root primordia. RNA was extracted using an RNeasy Plant Mini kit (Qiagen, Germany) according to the manufacturer's instructions. The quality and quantity of RNA were analyzed using an Agilent Bioanalyzer (Agilent Technologies, USA) and a Nanodrop (Thermo Fisher Scientific, USA), respectively. The cDNA synthesis was performed with NuGEN's Applause 3'Amp System (NuGEN, USA) according to the

manufacturer's instructions. NuGEN's Encore Biotin Module (NuGEN) was used to fragment the cDNA. Hybridization, washing, and scanning were performed according to the Affymetrix 30 Gene Chip Expression Analysis Technical Manual (Affymetrix, USA). Three chips were hybridized for both Col-0 and *rbohD/F* infected samples, with each microarray representing an independent biological replicate. The primary data analysis was performed with the Affymetrix Expression Console v1 software using the MAS5 algorithm. Affymetrix.CDF and .CEL files were loaded into the Windows GUI program RMAExpress (http://rmaexpress.bmbolstad.com/) for background correction, normalization (quantile), and summarization (median polish). After normalization, the computed robust multichip average (RMA) expression values were exported as a log scale to a text file. Probe set annotations were performed by downloading Affymetrix mapping files matching array element identifiers to AGI loci from the ARBC (http://www.arabidopsis.org). The genes with a fold change >1.5 and FDR value <5% were selected for enrichment analysis in GO (Gene Ontology) annotations of the domain 'biological process'**.** Microarray data for Col-0 plants have been published previously (Mendy *et al*., 2017).

Light microscopy

Arabidopsis wild-type Col-0 and mutant *rbohD/F* and *wat1* plants were grown and inoculated as described above. Samples consisting of root segments and attached juveniles were collected at 2 and 14 dpi. They were fixed and embedded in epoxy resin as described previously (Siddique *et al*., 2012) and sectioned on a Leica RM2165 microtome (Leica Microsystems, Germany). After staining with hot 0.1% (w/v) toluidine blue, the samples were examined under an Olympus AX70 "Provis" (Olympus, Japan) light microscope equipped with an Olympus DC90 digital camera. The obtained images were equalized for similar contrast and brightness using Adobe Photoshop software.

Validation of microarray chip data

To validate the microarray expression data, the top four down-regulated genes were selected. The samples were collected in the same manner as for the microarray analysis. RNA was extracted using an RNeasy Plant Mini kit (Qiagen, Germany) according to the manufacturer's instructions. cDNA was synthesized using a High Capacity cDNA Reverse Transcription Kit (Life Technologies, cat.no. 4368814, Country), according to the manufacturer's instructions. The transcript abundance of targeted genes was analyzed using the Stepone Plus Real-Time PCR System (Applied Biosystems, USA). Each sample contained 10 µL of Fast SYBR Green qPCR Master Mix with uracil-DNA, glycosylase, and 6-carboxy-x-rhodamine (Invitrogen, Country); 0.5 µL of forward primer; 0.5 µL of reverse primer (10 µM); 1 µL of cDNA; and water in 20 µL of total reaction volume. Samples were analyzed in three technical replicates. *18S* and *ACT2* genes were

used as internal controls. Relative expression was calculated as described previously (Pfaffl *et al.,* 2001) by which the expression of the target gene was normalized to *18S* to calculate fold change. All primer sequences are listed in Table S1.

SA, JA, and ABA quantification

Three days after inoculation with *H. schachtii*, short root segments containing sedentary nematodes and their associated syncytia were marked. The infected region around the nematode was then dissected, collected in liquid N_2, homogenized, and stored at −80°C. Care was taken not to collect any tip or lateral root primordia. Corresponding root segments (excluding root tips and lateral root primordia) from uninfected plants were collected as a control. The material was homogenized using liquid N_2 and extracted at −80°C using the modified Bieleski solvent (Van Meulebroek *et al*., 2012). After filtration and evaporation, chromatographic separation was performed on a U-HPLC system (Thermo Fisher Scientific, USA) equipped with a Nucleodur C18 column (50 x 2 mm; 1.8 µm) and using a mobile phase gradient consisting of acidified methanol and water. Mass spectrometry analysis was conducted in selected-ion monitoring (SIM) mode with a Q Exactive Orbitrap mass spectrometer (Thermo Fisher Scientific, USA), operating in both positive and negative electrospray ionization mode at a resolution of 70,000 full width at half maximum (Yimer *et al*., 2018).

IAA quantification

Three days after inoculation with *H. schachtii*, short root segments containing sedentary nematodes and their associated syncytia were marked. The infected region around the nematode was then dissected, collected in liquid N_2, homogenized, and stored at −80°C. Care was taken not to collect any tip or lateral root primordia. Corresponding root segments (excluding root tips and lateral root primordia) from uninfected plants were collected as a control. Indole acetic acid (IAA) was quantified according to Nakamura *et al.* (2013) with the only difference that D5-IAA was used as an internal standard.

Constructs and stable plant transformants

The previously described binary vector *pmdc162-proWAT1:GUS* was used to create stably transformed *pWAT1:GUS* (Col-0 and *rbohD/F*) lines by floral dipping (Clough and Bent, 1998). Transformed seeds were selected on MS medium containing 25 µg mL^{-1} hygromycin. Three independent homozygous lines were selected for further analysis. Three *WAT1* promoter fragments (sequence in Fig. S10, see later) were synthesized by Genewiz LLC and cloned into pDONR207 (Invitrogen, Country). These fragments were then transferred into *pmdc162* (Curtis

and Grossniklaus, 2003) by LR reaction. *pmdc162pWAT1^{ROS1}:GUS*, *pmdc162pWAT1^{ROS2}:GUS*, and *pmdc162WAT1^{ros1}:GUS* were introduced into *Agrobacterium tumefaciens* strain GV3101 for floral-dip transformation of Arabidopsis (ecotype Col-0). Seeds were selected on KNOP medium containing 25 µg mL^{-1} hygromycin. To generate *pWAT1-n:WAT1*, the *WAT1* coding sequence with *MauBI* and *AscI* restriction sites was synthesized in PUC57 by Genewiz LLC. Then, *GUS* in *pmdc162* was replaced by the *WAT1* coding sequence by classical cloning with the help of double digestion with *MauBI* and *AscI* restriction enzymes (Thermo Scientific, USA), thus creating the vector *35S:WAT1*. The *35S* promoter was then replaced by three promoter fragments, thus creating *pWAT1^{ROS1}*, *pWAT1^{ROS2}:WAT1*, and *pWAT1^{ros1}:WAT1*. Constructs were introduced into *A. tumefaciens* strain GV3101 for floral-dip transformation of the Arabidopsis *wat1* mutant background. Seeds were selected on KNOP medium containing 25 µg mL^{-1} hygromycin. Three independent homozygous lines were selected for further analysis.

GUS staining

Homozygous lines were grown in Knop or MS medium and infected with cyst or root knot J2s nematodes to visualize the GUS expression in a time-course analysis. The infected or uninfected roots were incubated with X-gluc for 3–4 h at 37°C. After incubation, the reaction was stopped and samples were washed with 70% (v/v) ethanol. Staining was done at three different time points: 1, 3, and 5 dpi. The GUS-stained syncytia and galls were photographed with a Leica DM8.0 inverted microscope equipped with a Leica DMC4500 digital camera and LAS software (Leica Microsystems, Germany). Images were resized, cropped, and adjusted for similar brightness, contrast, and background using Abode Photoshop software.

Results

RbohD and RbohF promote parasitism in cyst nematodes but not root-knot nematodes

We were concerned that reduction in the number of female cyst nematodes in *rbohD/F* might be due to auto-activation of immune responses in these mutants under our experimental conditions. To rule this out, we tested *rbohD/F* plants with the root-knot nematode *Meloidogyne incognita* as well as with the cyst nematode *Heterodera schachtii*. We grew plants in agar medium, and when the roots had spread throughout the medium, we inoculated plants with cyst or root-knot nematodes. As previously observed (Siddique *et al*., 2014), *rbohD/F* plants showed an 80% reduction in the number of female cyst nematodes at 14 days post inoculation (dpi) compared to wild-type plants (Col-0) (Fig. 1A). Average sizes of adult cyst nematode females and their syncytia were also significantly reduced in *rbohD/F* as compared to Col-0 (Fig. 1B and 1C). However, *rbohD/F* plants were significantly more susceptible to root-knot nematodes compared

with Col-0 as measured by the number of galls (Fig. 1D and Teixeira *et al*., 2016). The average diameter of the gall did not differ significantly between Col-0 and *rbohD/F*. These data suggest that RbohD and RbohF play a role in promoting plant susceptibility to cyst nematodes but not to root-knot nematodes.

RbohD and RbohF influence indole metabolism to promote cyst nematode parasitism

To identify target genes acting downstream of ROS that promote cyst nematode infection, we cut hundreds of tiny root segments (0.1 cm) and performed a comparative transcriptomic study (Fig. S1) between Col-0 and *rbohD/F* infected plants at 10 hours after cyst nematode inoculation (hai). This time point reflects the initial stages of nematode infection as concluded from an earlier study (Kammerhofer *et al*., 2015). Total RNA was extracted, labelled, and amplified to hybridize with the GeneChip Arabidopsis ATH1 Genome (Affymetrix UK Ltd). The ATH1 Genome Array contains more than 22,500 probe sets representing approximately 24,000 genes. Our results indicated that approximately 6,000 genes were differentially regulated (Fold change >2.0 and FDR value <5%) between Col-0 and *rbohD/F* infected root segments (Table S2). The functional categories that were particularly over-represented among differentially regulated genes include “response to oxygen containing compound” and “response to stimulus” (Fig. S2). A striking feature of the transcriptome analysis included a strong decrease in transcript abundance for genes involved in indole metabolic pathways including auxin (IAA) biosynthesis, transport and signaling genes in *rbohD/F* compared with Col-0 after infection (Fig. 2A and Table S3). These results were validated by quantitative RT-PCR (Fig. S3).

To further explore these results, we cut hundreds of microscopic root segments infected by cyst nematodes at 3 dpi and compared the levels of four different hormones (salicylic acid, SA; jasmonic acid, JA; auxin, IAA; abscisic acid, ABA) between Col-0 and *rbohD/F.* We did not see any change in the levels of SA and ABA upon nematode infection (Fig. 2B and 2C). In comparison to SA and ABA, there was a significant increase in levels of IAA and JA upon infection (Fig. 2D and 2E). However, increase in JA levels did not differ between Col-0 and *rbohD/F* (Fig. 2E). Notably, IAA was significantly elevated in infected Col-0 roots, whereas it remained at a similar level in control and infected *rbohD*/*F* roots compared to Col-0 roots (Fig. 2D).

Cyst nematodes fail to activate WAT1 in the absence of RbohD and RbohF

The gene that was most severely downregulated in *rbohD/F* plants relative to the wild type in our transcriptome analysis (fold change = −38.85) was *WALLS ARE THIN1* (*WAT1*), which encodes a vacuolar auxin transporter. WAT1 is a homolog of *Medicago truncatula Nodulin 21* (*MtN21*), which encodes a plant-specific integral membrane protein that is a member of the plant drug/metabolite exporter (P-DME) family (Ranocha *et al*., 2013). Although WAT1 has been detected in plasma membrane and vacuole fractions in two independent studies, recent analysis with the pro35S:WAT1-GFP construct demonstrated that WAT1 only localizes to the tonoplast (Ranocha et al., 2010). The loss-of-function mutant of *WAT1* confers broad-spectrum resistance to vascular pathogens including the bacteria *Ralstonia solanacearum* and *Xanthomonas campestris* as well as the fungi *Verticillium dahliae* and *V. albo-atrum*. A detailed transcriptomic and metabolomics analyses suggested a general repression of indole metabolism in *wat1* (Denancé *et al*., 2013; Ranocha *et al*., 2013; Ranocha *et al*., 2010), including a strong decrease in transcript abundance for genes encoding the indole glucosinolate biosynthetic pathway, and reduced amounts of indole metabolites such as tryptophan, IAA and IGS.

Similar to analyses of *wat1*, our transcriptomic and hormone analyses of *rbohD/F* roots showed a general repression of indole metabolism, including no increase in IAA levels upon cyst nematode infection. This similarity in mutant phenotypes is consistent with *WAT1* functioning downstream of *RbohD/F* and prompted us to investigate the involvement of WAT1 in cyst nematode infection. First of all, we investigated whether WAT1 and RbohD regulate expression of a common set of genes. To that end, we compared the set of 225 genes that are differentially expressed in *wat1* (Ranocha et al., 2010) with the set of differentially regulated genes in *rbohD/F*. We found that 75 out of the 225 genes were commonly differentially expressed in *rbohD/F* and *wat1*. Notably, a number of these genes encode proteins that play a role in cell wall, auxin, and ethylene metabolism (Table S4).

Next, we assessed *WAT1* gene expression during different stages of nematode infection by evaluating its expression in previously published transcriptomic data (Jammes *et al.*, 2005; Szakasits *et al.*, 2009; Barcala *et al.*, 2010; Mendy *et al.*, 2017). We found that *WAT1* expression is significantly decreased in the syncytium induced by *H. schachtii* at 5 and 15 dpi (Szakasits *et al.*, 2009). However, there was no significant difference in *WAT1* expression levels in root segments containing giant cells or galls infected with the RKN.

To get a detailed insights into spatio-temporal expression pattern of *WAT1* upon cyst and root-knot nematode infection, we used a reporter line containing the *WAT1* promoter (2980-bp region upstream of the coding sequence) driving *GUS* gene expression (*pWAT1:GUS;* Ranocha *et al*., 2010). In general, we did not observe GUS staining in uninfected roots of both Col-0 and *rbohD/F* plants except for a slight background expression that was restricted to younger root

zones close to the tips (Ranocha et al., 2010; Fig. S4). In contrast to the uninfected root, a majority of infection zones (~75%) in infected roots exhibited a strong and specific GUS expression at 1 dpi (Fig. 3A and 3G). A similar strong GUS expression was detected at 3 and 5 dpi. However, a number of infection zones showing expression declined as the infection proceeded from 3 dpi onwards (Fig. 3B, 3C, 3G, 3H and 3I). This expression pattern coincides with the Rboh-mediated ROS production described earlier (Siddique *et al*., 2014). Remarkably, the *pWAT1:GUS* reporter showed either no staining or very low GUS staining in *rbohD/F* lines upon infection by cyst nematodes (Figure 3D-3I). In comparison to cyst nematodes, root-knot nematodes did not induce *pWAT1:GUS* expression during early stages of infection (1dpi) in Col-0 or *rbohD/F* plants (Fig. S5). However, GUS expression was occasionally detected in both plant lines at 3 and 5 dpi (Fig. S5 and S6). To determine if *WAT1* expression is induced by ROS, we incubated *pWAT1:GUS* plants directly in 20 mM H_2O_2 and monitored *GUS* expression after 1 h. Compared to incubation in water, H_2O_2-treated seedlings induced a strong *GUS* expression (Fig. S7*)*. These findings suggest that *WAT1* expression is induced during the initial stages of cyst nematode infection in an Rboh-dependent manner.

WAT1 promotes infection by cyst nematodes but not root-knot nematodes

We examined six genes that are most strongly downregulated in *rbohD/F* compared to Col-0 upon cyst nematode infection and for whose loss-of-function mutants were available (Fig. S8). Of these mutants, only *wat1* plants displayed a significant drop in susceptibility to cyst nematodes relative to Col-0 (Fig. 4A and Fig. S9). Next, we phenotyped plant roots by measuring the total root length at 12 dpi after counting the nematodes. We found that *wat1* had slightly shorter roots. However, this does not affect the infection phenotype for *wat1*, which still has a significantly reduced number of females per centimeter of root length (Fig. S10). The sizes of syncytia (Fig. 4B) and female nematodes (Fig. 4C) at 14 dpi were similarly reduced in *wat1* and *rbohD/F* plants compared to Col-0. Upon root-knot nematode infection, the average number of galls increased significantly in *rbohD/F* relative to *wat1* and Col-0 (Fig. 4D). However, there was no difference in infection severity (number and size of galls) between *wat1* and Col-0 (Fig.4D and 4E). These data reinforce our view that WAT1 is involved in susceptibility of plants to cyst nematodes.

Because differences in indole metabolism were implicated in nematode susceptibility during our earlier transcriptome analysis and WAT1 is involved in auxin transport, we compared IAA levels between Col-0 and *wat1*. Upon infection with cyst nematodes, IAA accumulated at 3

dpi in Col-0 (Fig. 4F). However, IAA levels were consistently low in *wat1* plants with and without infection. Overall, these results suggest that Rboh-mediated ROS specifically promote cyst nematode infection through *WAT1's* IAA modulating activity (Fig. 4F).

Microscopic examinations of infection showed that in Col-0 roots, most of the juveniles had established well-developed syncytia at 2 dpi, and only few vascular cylinder cells were destroyed during nematode migration (Fig. 5). By contrast, nematode invasion caused substantial destruction in the vascular cylinders of *wat1* and *rbohD/F* plants (Fig. 5). Consequently, most of the juveniles had not yet established syncytium in *wat1* and *rbohD/F* at 2 dpi. At 14 dpi, syncytium induced in *wat1* and *rbohD/F* contained fewer incorporated cells, which were less hypertrophied than elements forming syncytium in infected Col-0 roots. Additionally, both mutants showed fewer cell divisions contributing to the secondary cover tissue (periderm) surrounding the syncytium.

ROS motifs in the WAT1 promoter are required for activation

Our data show that *WAT1* is regulated by H_2O_2 and RbohD/F during cyst nematode infection, but the regulatory components that activate *WAT1* expression are not known. To identify cis-regulatory elements of this gene, we mined the 2,980 bp upstream of the *WAT1* coding sequence for the various ROS-responsive motifs as predicted previously (Petrov *et al*. 2012) and found 19 motifs in this promoter region (Fig. 6A). We split the *WAT1* promoter region into three fragments each containing the TATA box but a different number of predicted ROS-inducible motifs (Fig. S11): fragment 1 had 5 ROS-inducible motifs (*pWAT*^{ROS1}); fragment 2 had no ROS-inducible motif (*pWAT*^{ros1}); and fragment 3 had 14 ROS-specific motifs (*pWAT*^{ROS2}). We created stably transformed Arabidopsis lines containing GUS fusion constructs for these three promoter fragments in the Col-0 background and examined GUS expression. In uninfected roots, we did not detect any GUS expression in any of the three lines (Fig. S12); however, when infected with cyst nematodes, *pWAT*^{ROS1}*:GUS* and *pWAT*^{ROS2}*:GUS* showed GUS expression similar to that observed in *pWAT1:GUS*. Occurrence of GUS staining was reduced strongly for *pWAT*^{ros1}*:GUS* upon cyst nematode infection at all three time points (Fig. 6 and 7). A similar GUS expression pattern was observed in all three lines upon H_2O_2-treatment (Fig. S12). In comparison

to cyst nematodes, all three lines showed occasional GUS expression upon RKN infection which was similar to that observed in *pWAT1:GUS* (Fig. S6).

Next, we tested whether expressing the *WAT1* gene under control of any of the three promoter fragments (*pWAT^{ROS1}:WAT1*, *pWAT1^{ROS2}:WAT1*, and *pWAT1^{ros1}:WAT1*) could restore susceptibility of *wat1* to wild-type levels. We created stably transformed Arabidopsis lines driving the *WAT1* expression fusion constructs for these three promoter fragments in the *wat1* background and performed nematode infection assays. We found that *pWAT^{ROS1}:WAT1* or *pWAT^{ROS2}:WAT1* restored *wat1* cyst nematode susceptibility to Col-0 levels, whereas *pWAT^{ros1}:WAT1* did not (Figure 8A-C). These data suggested that promoter fragments with the presence of ROS-responsive motifs activates *WAT1* expression upon cyst nematode infection.

Constitutive *WAT1* expression rescues the *rbohD* phenotype

We hypothesized that constitutive expression of *WAT1* might increase the susceptibility of *rbohD/F* to cyst nematodes. After several unsuccessful attempts to produce *rbohD/F* mutants with *35S:WAT1*, we continued with the single *rbohD* mutant. We selected two homozygous transgenic *rbohD* lines constitutively expressing *WAT1* (*35S:WAT1/rbohD-L1* and *35S:WAT1/rbohD-L2*; Fig. S13) for further experiments. We did not observe any phenotypic differences between the transgenic lines and Col-0 controls, yet the average number of female nematodes developing on *35S:WAT1/rbohD-L1* and *35S:WAT1/rbohD-L2* was higher than the number found on *rbohD* plants (Fig. 8D). However, the number of nematodes on the rescued lines was still lower than on Col-0, indicating a partial rescue of susceptibility. Furthermore, the average sizes of female nematodes and syncytia increased considerably for individuals developed on *35S:WAT1/rbohD-L1* and *35S:WAT1/rbohD-L2* compared to those found on *rbohD* lines, although they did not attain levels observed on wild-type plants (Fig. 8E and 8F). Taken together, these data reinforce the view that WAT1 acts downstream of RbohD/F and play an important in development and functioning of syncytium.

Discussion

In this study, we identified WAT1 as an essential component of the molecular mechanisms underlying RbohD/F-mediated susceptibility to cyst nematodes in plants. We first analyzed the expression of *WAT1* in response to cyst and root-knot nematode infection and found

commonalities, but also differences. We found that cyst nematode infection induces localized expression of *WAT1* in roots, which was strongly dependent on *RbohD/F*. This expression was particularly strong during the initial stages of infection suggesting a role for *WAT1* in syncytium initiation and establishment. Indeed, the reduced number of females, and the smaller size of females and syncytia in *wat1* plants underscored the importance of *WAT1* expression in cyst nematode parasitism. In comparison to cyst nematodes, we did not observe *WAT1* induction during the early stages of root-knot nematode infection. However, GUS expression was occasionally detected in both Col-0 and *rbohD/F* lines at 3 and 5dpi.

Root-knot nematode infection of *rbohD/F* produced an increase in average number of galls relative to Col-0 (Teixeira et al., 2016) corroborating a previously demonstrated antimicrobial role for Rboh-mediated ROS, but contrast with our finding that Rbohs play a role in promoting susceptibility to cyst nematodes. However, this dual role of Rbohs can be explained by differences in *WAT1* expression. While infection by cyst nematodes triggered a consistent increase in *WAT1* expression, infection by root-knot nematodes failed to do so. In line with these observations, *wat1* plants showed no change in susceptibility to root-knot nematode infection. We speculate that the difference in *WAT1* expression is likely due to a spatio-temporal difference in the ROS production upon cyst nematode versus root-knot nematode infection. A more detailed study will be needed to investigate the changes in ROS production during different stages of cyst and root-knot nematode infection.

Previous transcriptomic and metabolomics analyses suggested a general repression of indole metabolism in *wat1* (Denancé *et al*., 2013; Ranocha *et al*., 2013; Ranocha *et al*., 2010), which may explain the plethora of phenotypes in *wat1* mutants. Resistance to pathogens is mediated by an increase in SA contents, whereas decreased tryptophan/IAA content is responsible for reduced thickness of stem fibers cell walls. We propose that the Rboh-mediated increase in *WAT1* expression is essential for optimal channelization of indole metabolites, including tryptophan and IAA, in infected cells. This reprogramming of indole metabolites is imperative for the formation and functioning of syncytia. In the absence of ROS in the *rbohD/F* mutant, *WAT1* expression is severely downregulated in an infection-specific manner (Fig. 9). This downregulation of *WAT1* results in the suppression of indole metabolism causing a failure to induce a feeding site (caused by a lack of IAA accumulation) and poor development of syncytia/nematodes (caused by a lack of IAA accumulation and the activation of SA responses). Such transport-based modulation of the IAA metabolism has previously been demonstrated for other auxin transporters, such as PIN5 and PIN8, that mediate auxin flow at the ER membrane (Ding *et al*., 2012; Mravec et *al*., 2009). As further support for our hypothesis, previous analyses have demonstrated that both SA and auxin are important in the induction and function of

syncytium. For example, SA-deficient mutants (*sid2-1*, *pad4-1*, and NahG) have been shown to exhibit increased susceptibility to cyst nematodes (Wubben et al., 2008). In contrast, mutants that are deficient in auxin or auxin signaling revealed a significant decrease in susceptibility to both cyst and root-knot nematodes (Goverse *et al*., 2009; Grunewald *et al*., 2009; Karczmarek *et al*., 2004; Kyndt *et al*., 2014).

The *rboh* mutant plants hyperaccumulate SA, ethylene, and antimicrobial compounds in above-ground tissues upon pathogen challenge (Torres *et al*., 2017; Kadota *et al*., 2014; Pogány *et al*., 2009;), leading to the widely accepted belief that accumulation of these compounds is responsible for the reduced susceptibility of *rboh* mutants. However, the mechanism underlying accumulation of these compounds in *rbohD/F* remains unknown. One hypothesis is that key plant immune regulators, including Rbohs, are guarded by NLR proteins (nucleotide-binding domain and leucine-rich repeat-containing receptor), that auto-activate immune responses in mutants that are deficient in Rbohs (Kadota *et al*., 2015). Our data do not support the notion of an NLR-mediated reduction in susceptibility of *rbohD/F* to various pathogens, in particular to cyst nematodes. Instead, they demonstrate a unique role of RbohD/F-mediated ROS as a susceptibility factor in directing host metabolism to promote infection. Our results also establish WAT1 as an essential component of metabolic pathways linking oxidative burst signals to diverse downstream responses.

Our findings expand the known roles of Rboh in plant growth and immunity (Miller *et al*., 2009; Foreman et al., 2003; Kwak *et al*., 2003) by providing details of a unique mechanism that enables parasites to use host NADPH oxidase-mediated ROS for their own benefit. Determining whether nematodes actively release substances (i.e., effectors) to stimulate host ROS production will be a next step in our emerging understanding of host-parasite interactions.

Acknowledgments: We thank Stephan Neumann and Gisela Sichtermann for nematode maintenance. We very much appreciate Deborah Goffner and Philippe Ranocha for providing multiple batches of *wat1-1*, *wat1-3* seeds and pMDC32-WAT1 plasmid (= 2x35S-WAT1). This work was supported by a research grant from German Research Foundation to SSiddique (SI 1739/2-1) and an additional grant from USDA (CA-D-ENM-2562-RR). M. Shamim Hasan was supported by a stipend from German Academic Exchange Service (91525252).

Author contributions: SSiddique conceptualized the study and acquired the funding. MSH, DC, SV-M, SJ, MS, CM, SSzumski, BM and OC performed experiments. MSH, DC, MS, AN, FMWG and SSiddique analyzed the data. TK and AM performed hormone measurements. DC curated

the data and performed the statistics. SSiddique and DC wrote the original draft. All authors contributed to editing of manuscript. DC and MSH contributed equally to this work.

Data availability: The paper contain microarrays data and it is publicly available through array express under accession E-MTAB-10625. Raw data for infection assays is provided in Table S5. All transgenic lines are available upon request.

References

Asai, S., Yoshioka, H. (2009) Nitric oxide as a partner of reactive oxygen species participates in disease resistance to necrotrophic pathogen *Botrytis cinerea* in *Nicotiana benthamiana*. *Mol Plant Microbe Interact* **22**: 619-629.

Clough, S.J., Bent, A.F. (1998) Floral dip: a simplified method for Agrobacterium-mediated transformation of *Arabidopsis thaliana*. *Plant J* **16**: 735-743.

Curtis, M.D., Grossniklaus, U. (2003) A Gateway cloning vector set for high-throughput functional analysis of genes in planta. *Plant Physiol* **133**: 462-469.

Daudi, A., Cheng, Z., O'Brien, J.A., Mammarella, N., Khan, S., Ausubel, F.M., Bolwell, G.P. et al. (2012) The apoplastic oxidative burst peroxidase in Arabidopsis is a major component of pattern-triggered immunity. *Plant Cell* **24:** 275-287.

Delaney, T. P., Uknes, S., Vernooij, B., Friedrich, L., Weymann, K., Negrotto, D., Gut-Rella, M., Kessmann, H., Ryals, E. W. J. (1994) A central role of salicylic acid in plant-disease resistance. *Science* **266**: 1247-1250.

Denancé, N., Ranocha, P., Oria, N., Barlet, X., Rivière, M. P., Yadeta, K.A., Hoffmann, L., Perreau, F., Clement, G., Maria-Grondard A., et al. (2013) Arabidopsis *wat1* (*walls are thin1*)-mediated resistance to the bacterial vascular pathogen, *Ralstonia solanacearum*, is accompanied by cross-regulation of salicylic acid and tryptophan metabolism. *Plant J* **73**: 225-239.

Ding, Z., Wang, B., Moreno, I., Dupláková, N., Simon, S., Carraro, N., Reemmer, J., Pencik, A., Chen, X., Tejos, R., et al. (2012) ER-localized auxin transporter PIN8 regulates auxin homeostasis and male gametophyte development in Arabidopsis. *Nat Commun* **3**: 941.

Foreman, J., Demidchik, V., Bothwell, J. H., Mylona, P., Miedema, H., Torres, M. A., Linstead, P., Costa, S., Brownlee, C., Jones, J.D.g., et al. (2003) Reactive oxygen species produced by NADPH oxidase regulate plant cell growth. *Nature* **422**: 442-446.

Gheysen, G., Mitchum, M.G. (2018) Phytoparasitic nematode control of plant hormone pathways. *Plant Physiol* **179:** 1212-1226.

Goverse, A., Overmars, H., Engelbertink, J., Schots, A., Bakker, J. Helder, J. (2000) Both induction and morphogenesis of cyst nematode feeding cells are mediated by auxin. *Mol Plant Microbe Interact* **13**: 1121-1129.

Grunewald, W., Cannoot, B., Friml, J., Gheysen, G. (2009). Parasitic nematodes modulate PIN-mediated auxin transport to facilitate infection. *Plos Pathog* **5**: e1000266.

Ha, E.M., Oh, C.T., Bae, Y.S., Lee, W. (2005) A direct role for dual oxidase in Drosophila gut immunity. *Science* **310**: 847-850.

Holbein, J., Franke, R. B., Marhavý, P., Fujita, S., Górecka, M., Sobczak, M., Geldner, N., Schreiber, L., Grundler, F.M.W., Siddique, S. (2019). Root endodermal barrier system contributes to defence against plant-parasitic cyst and root-knot nematodes*. The Plant Journal* **100**, 221-236.

Kadota, Y., Shirasu, K., Zipfel, C. (2015) Regulation of the NADPH Oxidase RBOHD during plant immunity. *Plant Cell Physiol* **56**: 1472-1480.

Kadota, Y., Sklenar, J., Derbyshire, P., Stransfeld, L., Asai, S., Ntoukakis, V., Jones, J.D.G., Shirasu, K., Menke, F., Jones, A., Zipfel, C. (2014) Direct regulation of the NADPH oxidase RBOHD by the PRR-associated kinase BIK1 during plant immunity. *Mol Cell* **54**: 43-55.

Kammerhofer, N., Radakovic, Z., Regis, J. M., Dobrev, P., Vankova, R., Grundler, F.M.W., et al. (2015) Role of stress-related hormones in plant defense during early infection of the cyst nematode *Heterodera schachtii* in Arabidopsis. *New Phytol*, **207**: 778-789.

Karczmarek, A., Overmars, H., Helder, J., Goverse, A. (2004) Feeding cell development by cyst and root-knot nematodes involves a similar early, local and transient activation of a specific auxin-inducible promoter element. *Mol Plant Pathol* **5**: 343-346.

Kyndt, T., Goverse, A., Haegeman, A., Warmerdam, S., Wanjau, C., Jahani, M., ... & Gheysen, G. (2016). Redirection of auxin flow in Arabidopsis thaliana roots after infection by root-knot nematodes. *Journal of Experimental Botany*, **67**, 4559-4570.

Kwak, J. M., Mori, I.C., Pei, Z.M., Leonhardt, N., Torres, M.A., Dangl, J.L., Bloom, R.E., Bodde, S., Jones, J.D.G., Schroeder, J.I. (2003) NADPH oxidase *AtrbohD* and *AtrbohF* genes function in ROS-dependent ABA signaling in *Arabidopsis*. *EMBO J* **22**: 2623-2633.

Marhavý, P., Kurenda, A., Siddique, S., Tendon D.V., Zhou, F., Holbein, J., Shamim, M. H., Grundler F.M.W., Farmer E., Geldner, N. (2019). Single-cell damage elicits regional, nematode-restricting ethylene responses in roots. *The EMBO journal*, **38**, e100972.

Marino, D., Dunand, C., Puppo, A., Pauly, N. (2012) A burst of plant NADPH oxidases. *Trends Plant Sci* **17:** 9-15.

Mendy, B., Wang'ombe, M.W., Radakovic, Z.S., Holbein, J., Ilyas, M., Chopra, D., et al. (2017) Arabidopsis leucine-rich repeat receptor-like kinase NILR1 is required for induction of innate immunity to parasitic nematodes. *Plos Pathog* **13**: e1006284.

Miller, G., Schlauch, K., Tam, R., Cortes, D., Torres, M.A., Shulaev, V., et al. (2009) The plant NADPH oxidase RBOHD mediates rapid systemic signaling in response to diverse stimuli. *Sci Signal* **2**: ra45.

Mravec, J., Skůpa, P., Bailly, A., Hoyerová, K., Křeček, P., Bielach, A., Petrasek, J., Zhang, J., Gaykova, V., Stierhof, Y-D., et al. (2009) Subcellular homeostasis of phytohormone auxin is mediated by the ER-localized PIN5 transporter. *Nature* **459**: 1136-1140.

Nakamura, Y., Reichelt, M., Mayer V.E, Mithöfer A. (2013) Jasmonates trigger pre induced formation of 'outer stomach' in carnivorous sundew plants. *Proc R Soc* 280: 20130228.

Nicol, J.M., Turner, S.J., Coyne, D.L., Den Nijs, L., Hockland, S., Maafi, Z.T. (2011) Current nematode threats to world agriculture, in: *Genomics and Molecular Genetics of Plant-Nematode Interactions,* J. Jones, G. Gheysen, C. Fenoll, Eds. (Springer Netherlands, Dordrecht, 2011), pp: 21-43.

Petrov, V., Vermeirssen, V., De Clercq, I., Van Breusegem, F., Minkov, I., Vandepoele, K., Gechev, T. S. (2012). Identification of cis-regulatory elements specific for different types of reactive oxygen species in *Arabidopsis thaliana*. *Gene*: ***499***: 52-60.

Pfaffl, M. W. (2001) A new mathematical model for relative quantification in real-time RT-PCR. *Nucleic Acids Res* **29**: e45.

Pogány, M., von Rad, U., Grün, S., Dongó, A., Pintye, A., Simoneau, P., Bahnweg, G., Kiss, L., Barna, B., Durner, J., et al. (2009) Dual roles of reactive oxygen species and NADPH oxidase RBOHD in an Arabidopsis-*Alternaria* Pathosystem. *Plant Physiol* **151:** 1459-1475.

Proels, R. K., Oberhollenzer, K., Pathuri, I. P., Hensel, G., Kumlehn, J., Hückelhoven, R. (2010) RBOHF2 of barley is required for normal development of penetration resistance to the parasitic fungus *Blumeria graminis* f. sp *hordei*. *Mol Plant Microbe Ineract* **23**: 1143-1150.

Ranocha, P., Dima, O., Nagy, R., Felten, J., Corratgé-Faillie, C., Novák, O., Morreel, K., Lacombe, B., Martinez, Y., Pfrunder, S., et al. (2013) Arabidopsis *WAT1* is a vacuolar auxin transport facilitator required for auxin homoeostasis. *Nat Commun* **4**: 2625.

Ranocha, P., Denancé, N., Vanholme, R., Freydier, A., Martinez, Y., Hoffmann, L., Kohler, L., Pouzet, C., Renou, J-P., Sundberg, B., Boerjan, W., Goffner, D., et al. (2010) *Walls are thin 1* (*WAT1*), an Arabidopsis homolog of *Medicago truncatula NODULIN21*, is a tonoplast-localized protein required for secondary wall formation in fibers. *Plant J* **63**: 469-483.

Shah, S.J., Anjam, M.S., Mendy, B., Anwer, M.A., Habash, S.S., Lozano-Torres, J.L., Grundler, F.M.W., Siddique, S. (2017) Damage-associated responses of the host contribute to defence against cyst nematodes but not root-knot nematodes. *J Exp Bot* **68**, 5949-5960 (2017).

Sijmons, P.C., Grundler, F.M.W., von Mende, N., Burrows, P.R., Wyss, U. (1991) *Arabidopsis-thaliana* as a new model host for plant-parasitic nematodes. *Plant J* **1**: 245-254.

Smant, G., Helder, J., Goverse, A. (2018) Parallel adaptations and common host cell responses enabling feeding of obligate and facultative plant parasitic nematodes. *Plant J* **93**, 686-702 (2018).

Siddique, S., Grundler, F.M.W. (2018) Parasitic nematodes manipulate plant development to establish feeding sites. *Curr Opin Microbiol* **46:** 102-108.

Siddique, S., Matera, C., Radakovic, Z.S., Hasan, M.S., Gutbrod, P., Rozanska, E., et al. *(2014)* Parasitic worms stimulate host NADPH Oxidases to produce reactive oxygen species that limit plant cell death and promote infection. *Sci Signal* **7**, ra33 (2014).

Siddique, S., Grundler, F.M.W. (2015) Metabolism in nematode feeding sites. *Adv Bot Res* **73**, 119-138 (2015).

Siddique, S., Sobczak, M., Tenhaken, R., Grundler, F.M.W., Bohlmann, H. (2012) Cell wall ingrowths in nematode induced syncytia require UGD2 and UGD3. *PLoS ONE* **7**: e41515.

Torres, D.P., Proels, R.K., Schempp, H., Huckelhoven, R. (2017) Silencing of *RBOHF2* causes leaf age-dependent accelerated senescence, salicylic acid accumulation, and powdery mildew resistance in barley. *Mol Plant Microbe Interact* **30**: 906-918.

Torres, M.A., Dangl, J.L. (2005) Functions of the respiratory burst oxidase in biotic interactions, abiotic stress and development. *Curr Opin Plant Biol* **8:** 397-403.

Torres, M.A., Dangl, J.L., Jones, J.D.G. (2002) Arabidopsis gp91^{phox} homologues *AtrbohD* and *AtrbohF* are required for accumulation of reactive oxygen intermediates in the plant defense response. *P Natl Acad Sci USA* **99:** 517-522.

Torres, M.A., Onouchi, H., Hamada, S., Machida, C., Hammond-Kosack, K.E., Jones, J.D.G., et al. (1998) Six *Arabidopsis thaliana* homologues of the human respiratory burst oxidase (*gp91^{phox}*). *Plant J* **14:** 365-370.

Trujillo, M., Altschmied, M., Schweizer, P., Kogel, K.H., Huckelhoven, R. (2006) Respiratory burst oxidase homologue A of barley contributes to penetration by the powdery mildew fungus *Blumeria graminis* f. sp *hordei*. *J Exp Bot* **57:** 3781-3791

Van Meulebroek, L., Bussche, J.V., Steppe, K., Vanhaecke, L. (2012) Ultra-high-performance liquid chromatography coupled to high resolution Orbitrap mass spectrometry for

metabolomic profiling of the endogenous phytohormonal status of the tomato plant. *Journal of Chromatography A* **1260**: 67– 80.

Yimer, H.Z., Nahar, K., Kyndt, T., Haeck, A., Van Meulebroek, L., Vanhaecke, L., Demeestere, K., Hofte, M., Gheysen, G. (2018) Gibberellin antagonizes jasmonate-induced defense against *Meloidogyne graminicola* in rice. *New Phytologist*, **218**, 646-660.

Supporting Information

Fig. S1: Schematic of microscopic samples for transcriptomic study between Col-0 and *rbohD/F* plants.

Fig. S2: GO enrichment among differentially regulated genes between Col-0 and *rbohD/F* at 10 hours post inoculation.

Fig. S3: Validation of transcriptome results.

Fig. S4: *pWAT1:GUS* expression in Col-0 and *rbohD/F* uninfected roots.

Fig. S5: WAT1 expression in response to root-knot nematode infection.

Fig. S6: Analysis of *pWAT1:GUS* expression upon root-knot nematode infection.

Fig. S7: WAT1 induction by H2O2.

Fig. S8: Cyst nematode assays for loss-of-function mutants for 6 significantly downregulated genes in *rbohD/F* as compared to Col-0 upon infection.

Fig. S9: WAT1 is required for cyst nematode infection.

Fig. S10: WAT1 is required for cyst nematode infection.

Fig. S11: Sequence of WAT1 Promoter fragments generated based on the presence or absence of cis regulatory ROS motifs.

Fig. S12: WAT1 induction by H2O2.

Fig. S13: Analysis of *WAT1* expression in Col-0, *rbohD*, and *35S:WAT1/rbohD* lines.

Table S1: Primer sequences used in this study.

Table S2: List of differentially regulated genes between Col-0 and rbohD/F at 10 hours post inoculation.

Table S3: Expression of genes involved in auxin biosynthesis, transport and signaling in rbohD/F compared with Col-0 10 hours post inoculation

Table S4: List of commonly differentiay expressed genes in rbohD/F and wat1.

Table S5: Raw data for infection assays

Figure 1: **RbohD and RbohF promote parasitism in beet cyst nematodes *Heterodera schachtii* but not root-knot nematodes *Meloidogyne incognita*.** (**A)** Average number of female cyst nematodes present per plant root system at 14 dpi. (**B**) Average size of plant syncytia at 14 dpi. (**C**) Average size of female nematodes at 14 dpi. (**D**) Average number of galls present per plant root system at 20 dpi. (**E**) Average size of galls at 21 dpi. (A to D) Experiments were performed at least three times independently with the same outcome. Data from one experiment are shown. Bars represent mean ± SE. Data were analyzed using t-test. Asterisks indicate significant differences compared to Col-0 ($P < 0.05$).

Figure 2: RbohD and RbohF regulate indole metabolism in response to *Heterodera schachtii* infection. (**A**) A heat map showing expression of genes involved in the indole metabolite pathway in *rbohD/F* compared to Col-0 upon cyst nematode infection. **(B to E)** The amount of SA (salicylic acid), ABA (abscisic acid), JA (jasmonic acid), and IAA (indole-3-acetic acid) in small segments of control and cyst nematode infected roots at 3 dpi. Bars represent mean ± SE of three to six independent replicates. Each replicate consists of hundreds of tiny root segments containing infection sites. Data were assessed using ANOVA ($P < 0.05$) and Tukey's HSD posthoc tests. Columns not sharing the same letter are significantly different from each other. C, Control; I, infected.

Figure 3: RbohD and RbohF regulate WAT1 expression in response to *Heterodera schachtii* infection. (A-F) *pWAT1:GUS* expression in Col-0 and *rbohD/F* roots at 1 (**A** and **D**), 3 (**B** and **E**) and 5 dpi (**C** and **F**). (**G-I**) Quantification of *pWAT1:GUS* expression in Col-0 and *rbohD/F* roots upon cyst nematode infection. Bars represent mean ±SE. Three independent experiments were performed, and data are the average for three experiments. Asterisks indicate statistically significant differences with Col-0 using t-test ($P < 0.05$). Arrowhead indicates nematodes. Scale bar corresponds to 100 µm.

Figure 4: WAT1 is required for *Heterodera schachtii* infection. (**A**) Average number of female cyst nematodes present per plant root system at 14 dpi. (**B**) Average size of female nematodes at 14 dpi. (**C**). Average size of plant syncytia at 14 dpi. (D) Average number of galls present per plant root system at 20 dpi. (**E**) Average size of galls at 21 dpi. (**F**) Amount of IAA in control and cyst nematode infected roots at 3 dpi measured by UPLC. (**A-D**) Experiments were performed three to four times independently with the same outcome. Data from one experiment are shown. (**E** and **F**) Mean ± SE for four independent biological replicates. Bars represent mean ± SE. Data

were assessed using single-factor analysis of variance (ANOVA, $P < 0.05$) and Tukey's HSD posthoc tests. Bars not sharing the same letter are significantly different from each other.

Figure 5: Cross sections of *Heterodera schachtii* infected root sections from Col-0, *wat1-1* and *rbohD/F* at 2 and 14 dpi. Arrows indicate nematode juveniles. Pd, periderm; S, syncytium. Scale bars correspond to 20 µm.

Figure 6: *Heterodera schachtii* activates the *WAT1* promoter containing ROS-responsive motifs. (**A**) The *WAT1* promoter was split into three fragments, $pWAT^{ROS1}$ with 5 ROS motifs, $pWAT1^{ROS2}$ with 14 ROS motifs, and $pWAT1^{ros1}$ with none. (**B-D**) Quantification of GUS expression driven by various promoter fragments in Col-0 roots upon cyst nematode infection. Bars represent mean ± SE obtained from three independent experiments. Data were subjected to ANOVA ($P < 0.05$) and Tukey's HSD posthoc analysis. Columns not sharing the same letter are significantly different from each other.

Figure 7: *Heterodera schachtii* activates the *WAT1* promoter. (A-H) GUS expression driven by promoter fragments as described in Fig. 6 in transformed Col-0 roots upon cyst nematode infection. Arrowheads point to nematodes. Scale bars correspond to 100 µm.

Figure 8: Minimum ROS motif promoter in the *wat1* mutant and constitutive expression of *WAT1* in *rbohD* mutant restore susceptibility to *Heterodera schachtii*. (**A**) Average number of female cyst nematodes present in a single root system at 14 dpi. (**B**) Average size of female nematodes at 14 dpi. (**C**) Average size of plant syncytia at 14 dpi. (**D**) Average number of female cyst nematodes present in a single root system at 14 dpi. (**E**) Average size of female nematodes at 14 dpi. (**F**) Average size of plant syncytia at 14 dpi. Bars represent mean ± SE. Data were assessed using single-factor analysis of variance (ANOVA, $P < 0.05$) and Tukey's HSD posthoc tests. Bars not sharing the same letter are significantly different from each other. Experiments were performed three times independently with same outcome. Data from one experiment are shown.

Figure 9: Scheme of the Rboh-mediated molecular network. *Heterodera schachtii* infection triggers RbohD/F mediated ROS production, which in turn activates WAT1 and promotes parasite infection by modulating indole metabolism. IAA, Indole-3-acetic acid, SA. Salicylic acid.

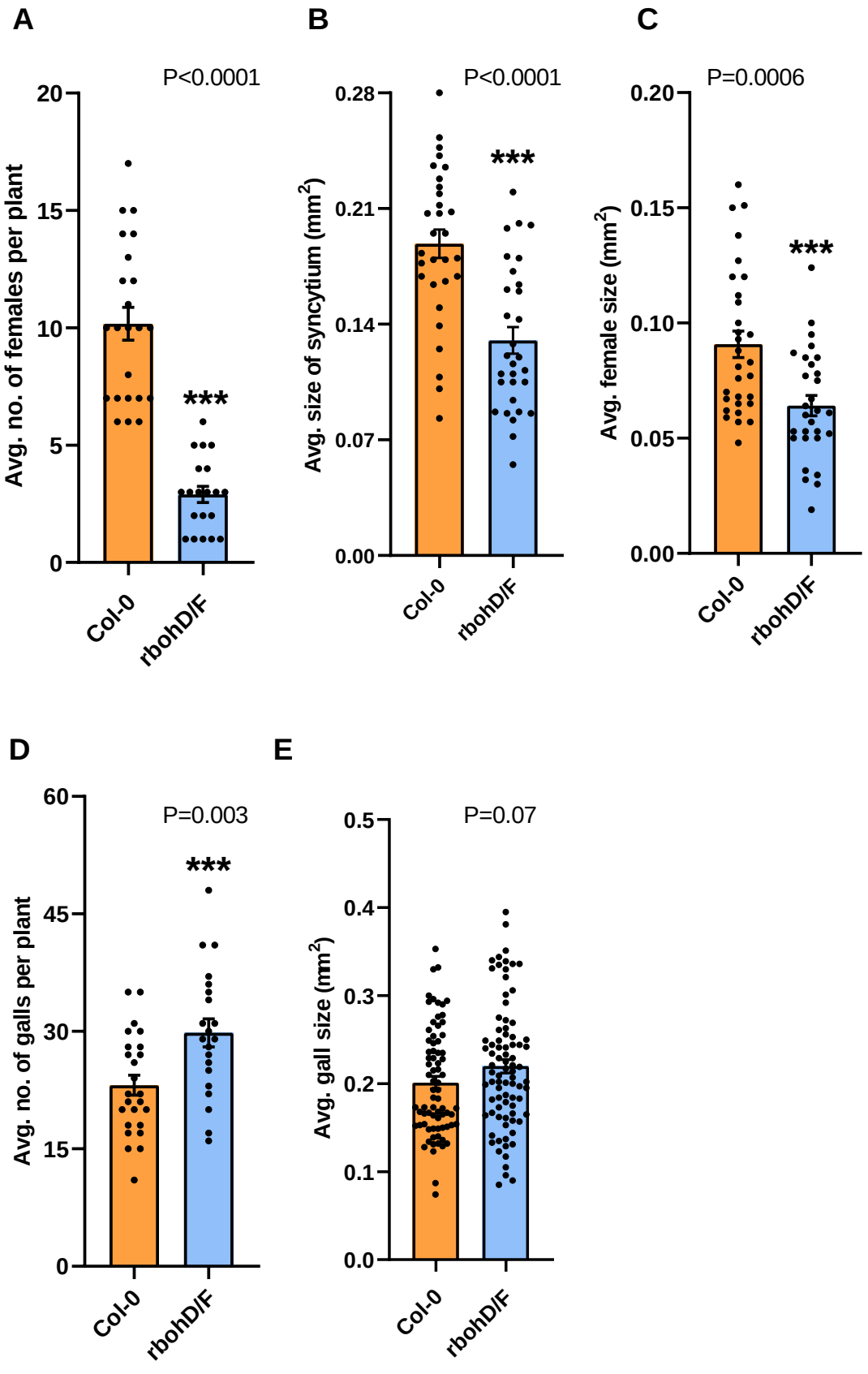
A
P<0.0001
Avg. no. of females per plant
20
15
10
5
0
***
Col-0
rbohD/F
B
P<0.0001
Avg. size of syncytium (mm2)
0.28
0.21
0.14
0.07
0.00
***
Col-0
rbohD/F
C
P=0.0006
Avg. female size (mm2)
0.20
0.15
0.10
0.05
0.00
***
Col-0
rbohD/F
D
P=0.003
Avg. no. of galls per plant
60
45
30
15
0
***
Col-0
rbohD/F
E
P=0.07
Avg. gall size (mm2)
0.5
0.4
0.3
0.2
0.1
0.0
Col-0
rbohD/F

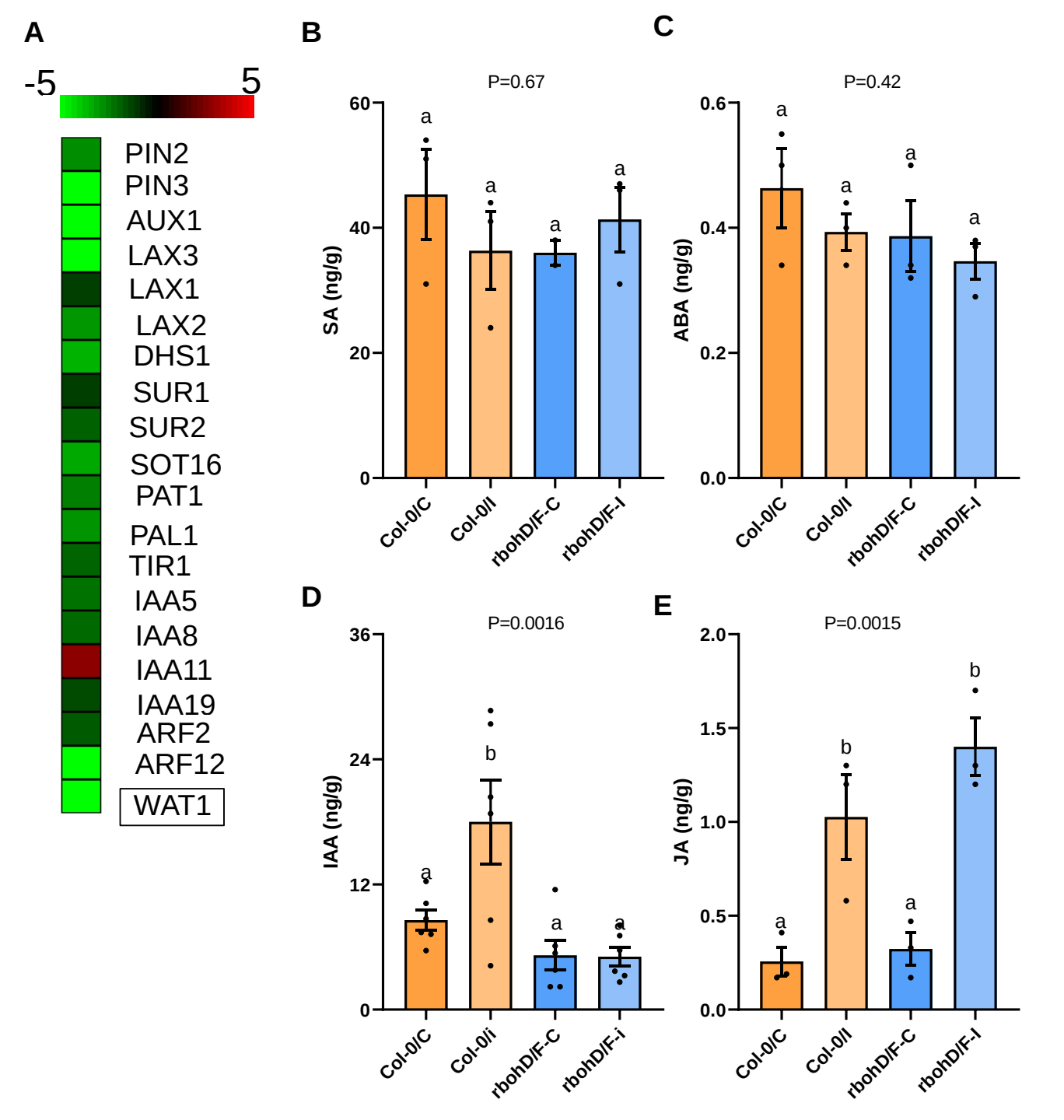
A
-5
5
PIN2
PIN3
AUX1
LAX3
LAX1
LAX2
DHS1
SUR1
SUR2
SOT16
PAT1
PAL1
TIR1
IAA5
IAA8
IAA11
IAA19
ARF2
ARF12
WAT1
B
P=0.67
SA (ng/g)
60
40
20
0
a
a
a
a
Col-0/C
Col-0/I
rbohD/F-C
rbohD/F-I
C
P=0.42
ABA (ng/g)
0.6
0.4
0.2
0.0
a
a
a
a
Col-0/C
Col-0/I
rbohD/F-C
rbohD/F-I
D
P=0.0016
IAA (ng/g)
36
24
12
0
a
b
a
a
Col-0/C
Col-0/i
rbohD/F-C
rbohD/F-i
E
P=0.0015
JA (ng/g)
2.0
1.5
1.0
0.5
0.0
a
b
a
b
Col-0/C
Col-0/I
rbohD/F-C
rbohD/F-I

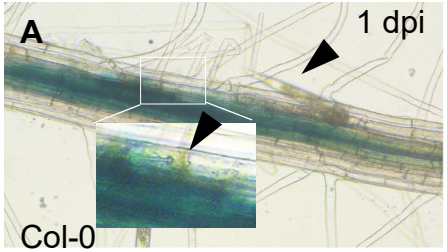
A
1 dpi
Col-0

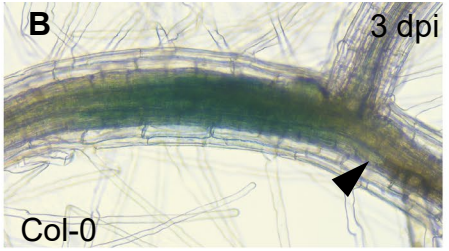
B
3 dpi
Col-0


C
5 dpi
Col-0

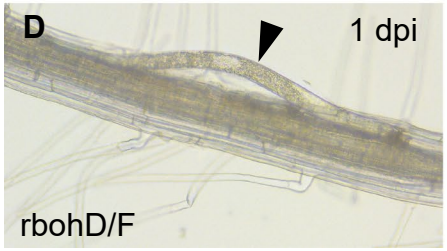
D
1 dpi
rbohD/F

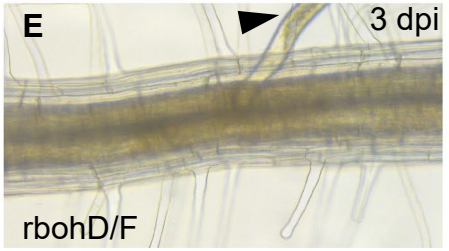
E
3 dpi
rbohD/F


F
5 dpi
rbohD/F

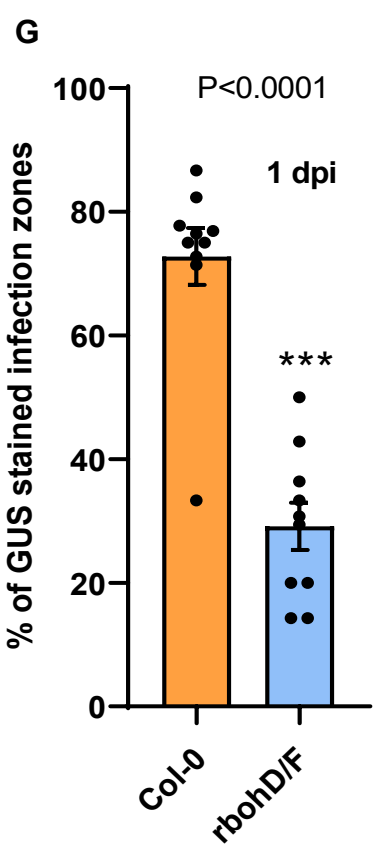
G
P<0.0001
1 dpi
***
% of GUS stained infection zones
100
80
60
40
20
0
Col-0
rbohD/F

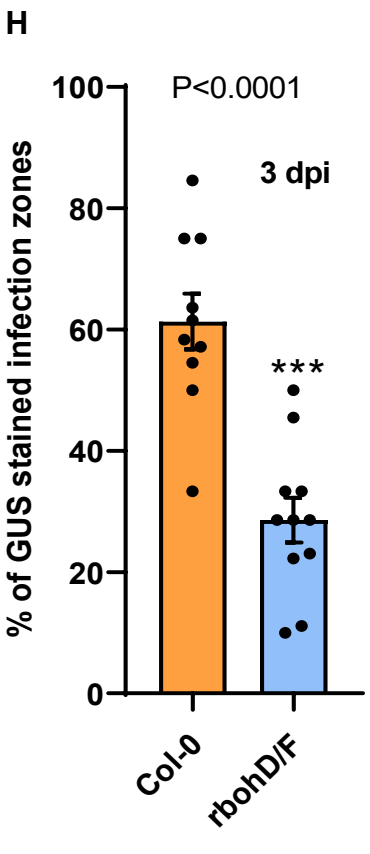
H
P<0.0001
3 dpi
***
% of GUS stained infection zones
100
80
60
40
20
0
Col-0
rbohD/F

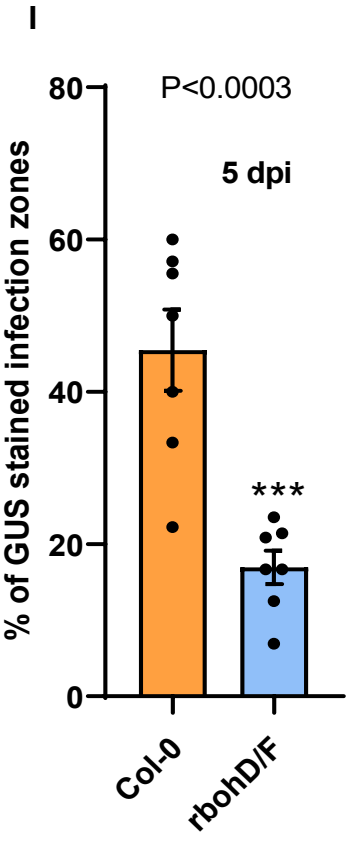
I
P<0.0003
5 dpi
***
% of GUS stained infection zones
80
60
40
20
0
Col-0
rbohD/F

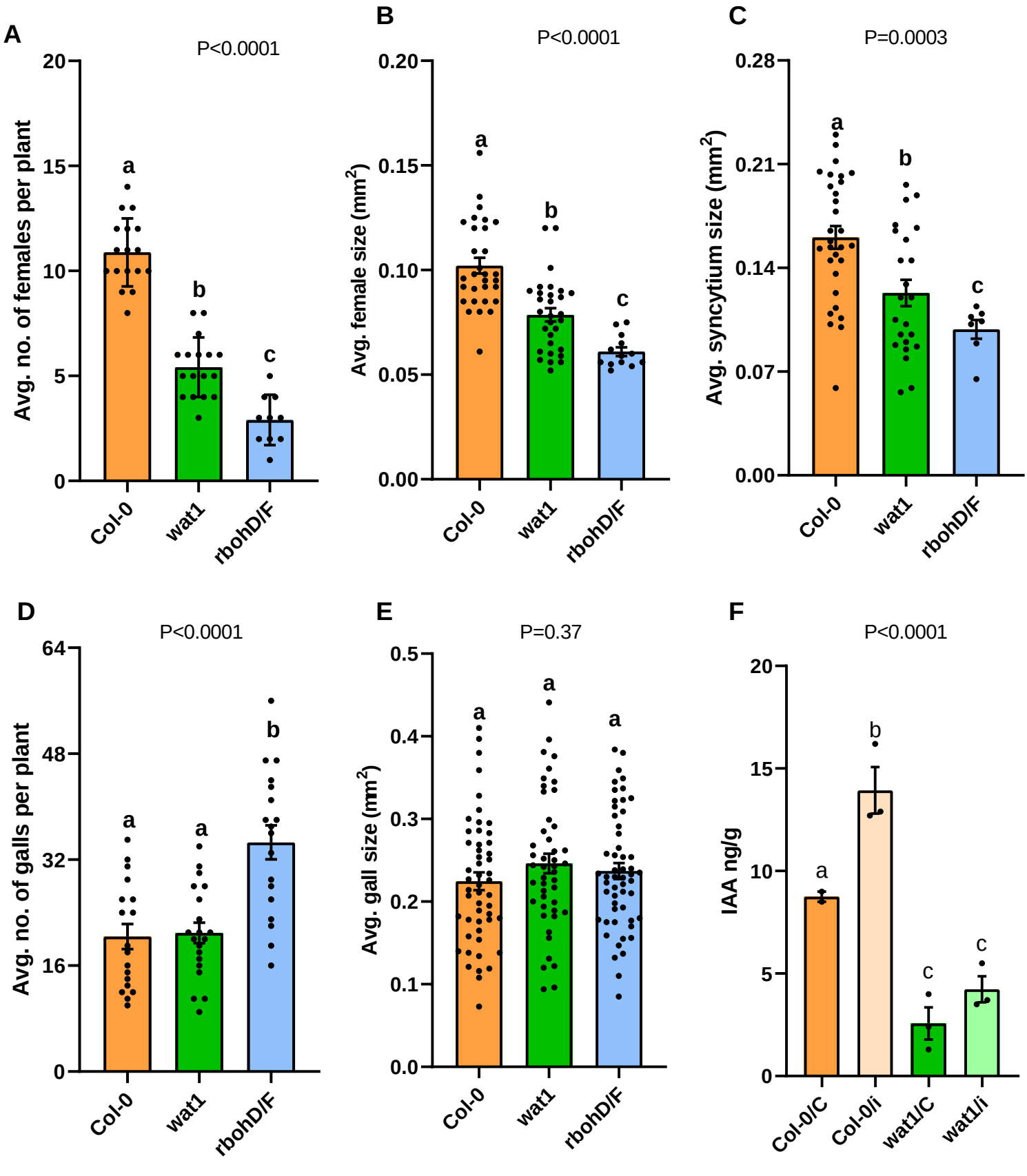
A
P<0.0001
Avg. no. of females per plant
20
15
10
5
0
a
b
c
Col-0
wat1
rbohD/F
B
P<0.0001
Avg. female size (mm2)
0.20
0.15
0.10
0.05
0.00
a
b
c
Col-0
wat1
rbohD/F
C
P=0.0003
Avg. syncytium size (mm2)
0.28
0.21
0.14
0.07
0.00
a
b
c
Col-0
wat1
rbohD/F
D
P<0.0001
Avg. no. of galls per plant
64
48
32
16
0
a
a
b
Col-0
wat1
rbohD/F
E
P=0.37
Avg. gall size (mm2)
0.5
0.4
0.3
0.2
0.1
0.0
a
a
a
Col-0
wat1
rbohD/F
F
P<0.0001
IAA ng/g
20
15
10
5
0
a
b
c
c
Col-0/C
Col-0/i
wat1/C
wat1/i

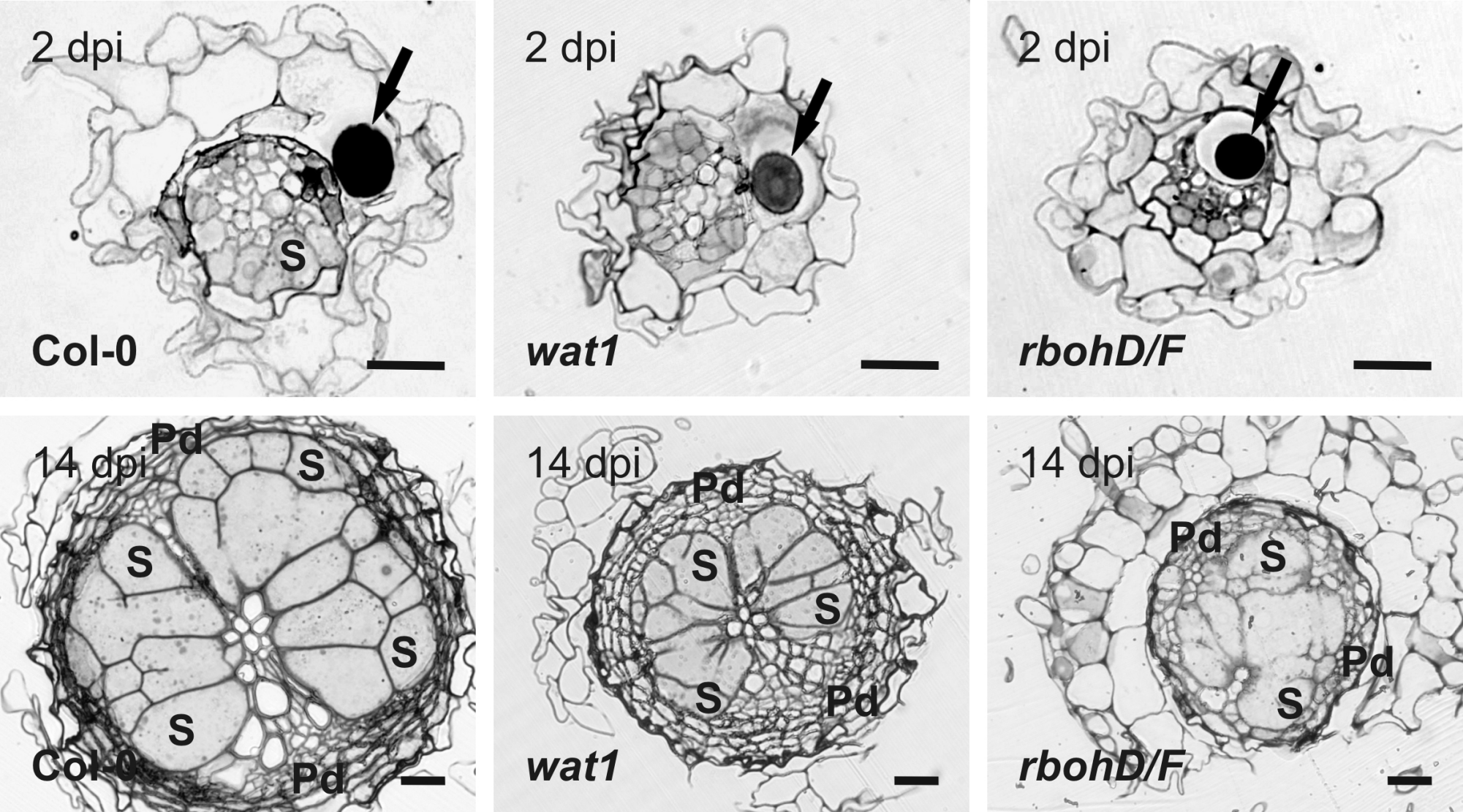
2 dpi
S
Col-0
2 dpi
wat1
2 dpi
rbohD/F
14 dpi
Pd
S
S
S
S
Pd
Col-0
14 dpi
Pd
S
S
S
Pd
wat1
14 dpi
Pd
S
Pd
S
Pd
rbohD/F

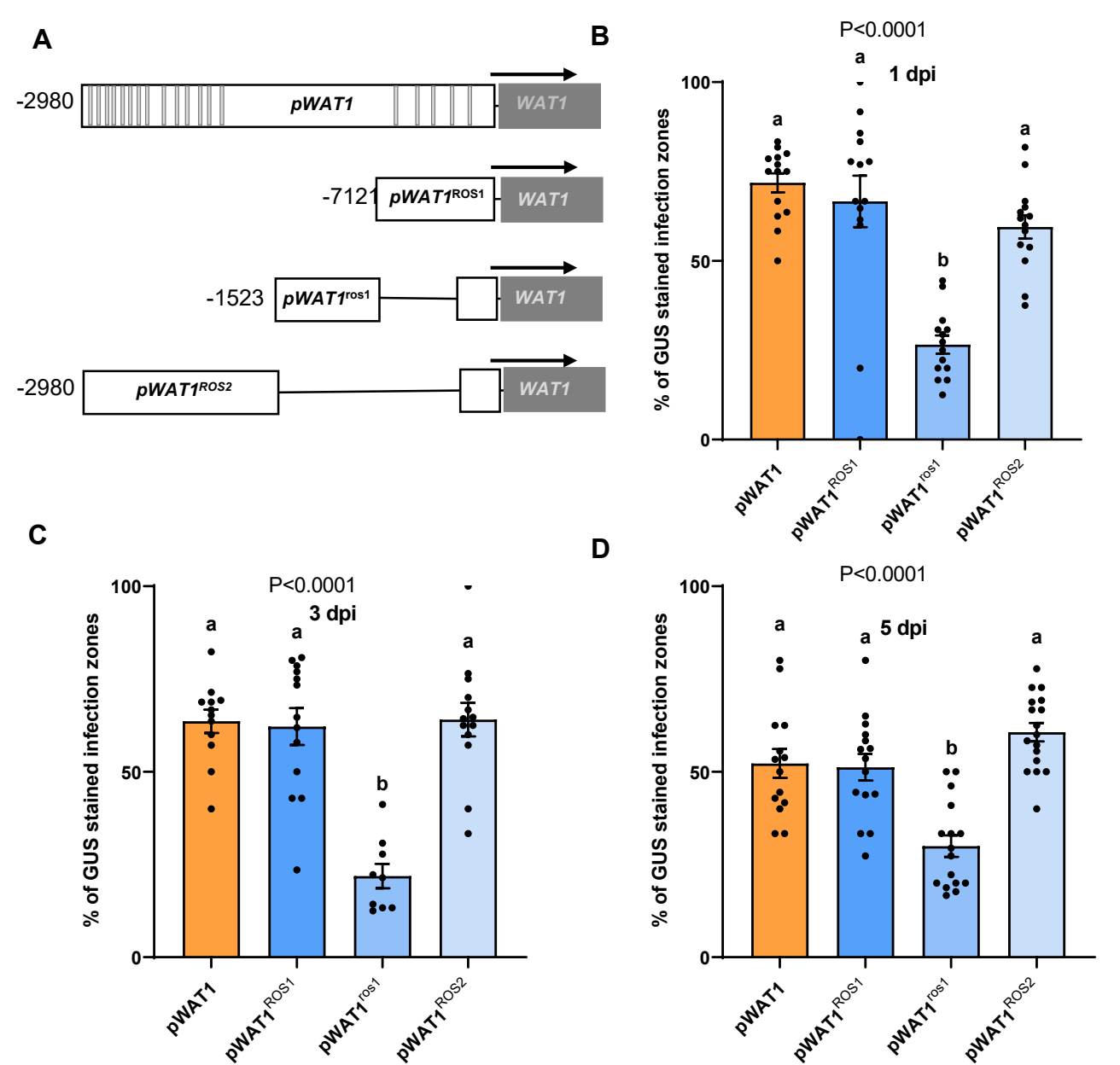
A
-2980
pWAT1
WAT1
-7121
pWAT1ROS1
WAT1
-1523
pWAT1ros1
WAT1
-2980
pWAT1ROS2
WAT1
B
P<0.0001
1 dpi
% of GUS stained infection zones
100
50
0
a
a
b
a
pWAT1
pWAT1ROS1
pWAT1ros1
pWAT1ROS2
C
P<0.0001
3 dpi
% of GUS stained infection zones
100
50
0
a
a
b
a
pWAT1
pWAT1ROS1
pWAT1ros1
pWAT1ROS2
D
P<0.0001
5 dpi
% of GUS stained infection zones
100
50
0
a
a
b
a
pWAT1
pWAT1ROS1
pWAT1ros1
pWAT1ROS2

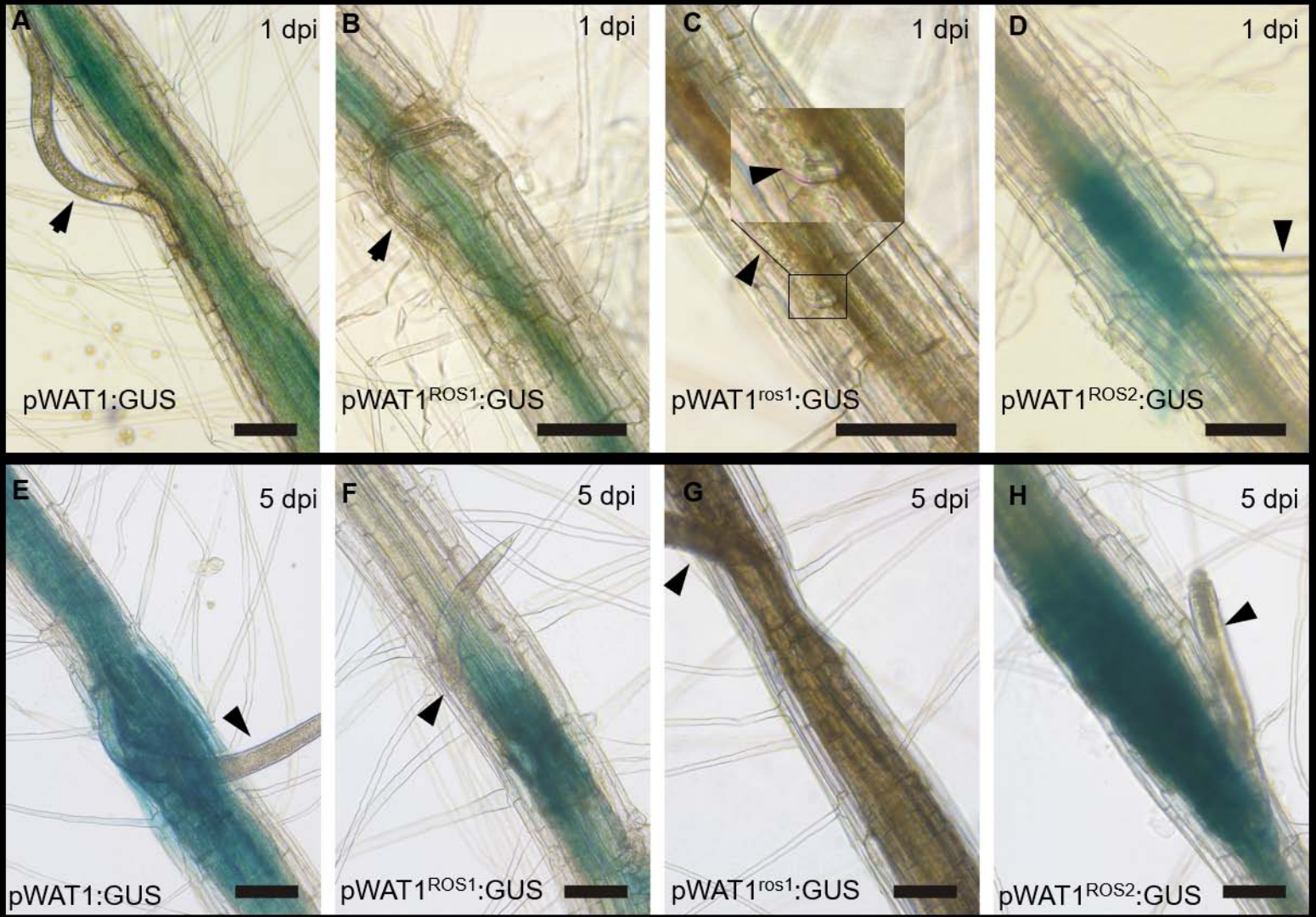
A
1 dpi
pWAT1:GUS
B
1 dpi
pWAT1ROS1:GUS
C
1 dpi
pWAT1ros1:GUS
D
1 dpi
pWAT1ROS2:GUS
E
5 dpi
pWAT1:GUS
F
5 dpi
pWAT1ROS1:GUS
G
5 dpi
pWAT1ros1:GUS
H
5 dpi
pWAT1ROS2:GUS

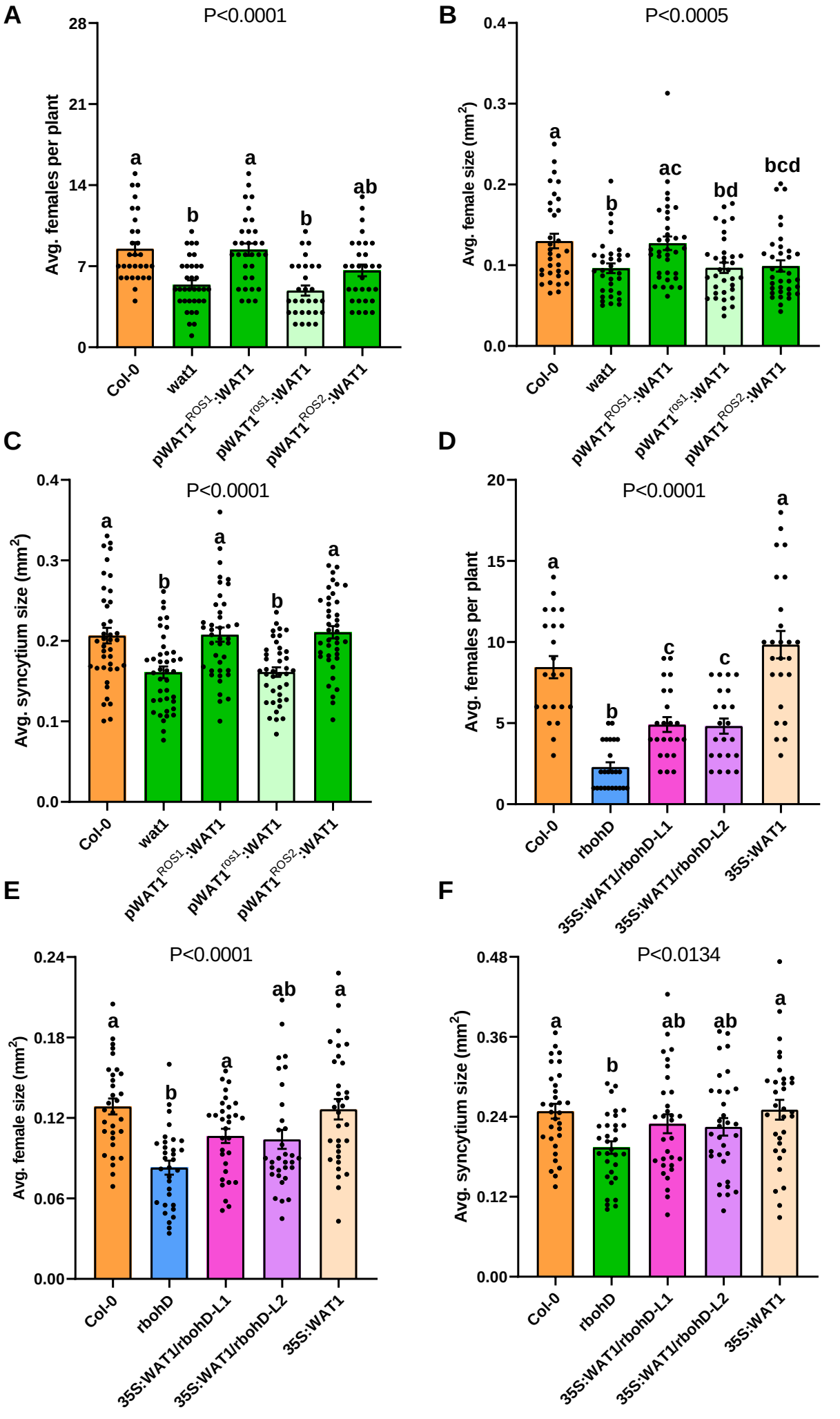
A
P<0.0001
Avg. females per plant
28
21
14
7
0
a
b
a
b
ab
Col-0
wat1
pWAT1ROS1:WAT1
pWAT1ros1:WAT1
pWAT1ROS2:WAT1
B
P<0.0005
Avg. female size (mm2)
0.4
0.3
0.2
0.1
0.0
a
b
ac
bd
bcd
Col-0
wat1
pWAT1ROS1:WAT1
pWAT1ros1:WAT1
pWAT1ROS2:WAT1
C
P<0.0001
Avg. syncytium size (mm2)
0.4
0.3
0.2
0.1
0.0
a
b
a
b
a
Col-0
wat1
pWAT1ROS1:WAT1
pWAT1ros1:WAT1
pWAT1ROS2:WAT1
D
P<0.0001
Avg. females per plant
20
15
10
5
0
a
b
c
c
a
Col-0
rbohD
35S:WAT1/rbohD-L1
35S:WAT1/rbohD-L2
35S:WAT1
E
P<0.0001
Avg. female size (mm2)
0.24
0.18
0.12
0.06
0.00
a
b
a
ab
a
Col-0
rbohD
35S:WAT1/rbohD-L1
35S:WAT1/rbohD-L2
35S:WAT1
F
P<0.0134
Avg. syncytium size (mm2)
0.48
0.36
0.24
0.12
0.00
a
b
ab
ab
a
Col-0
rbohD
35S:WAT1/rbohD-L1
35S:WAT1/rbohD-L2
35S:WAT1

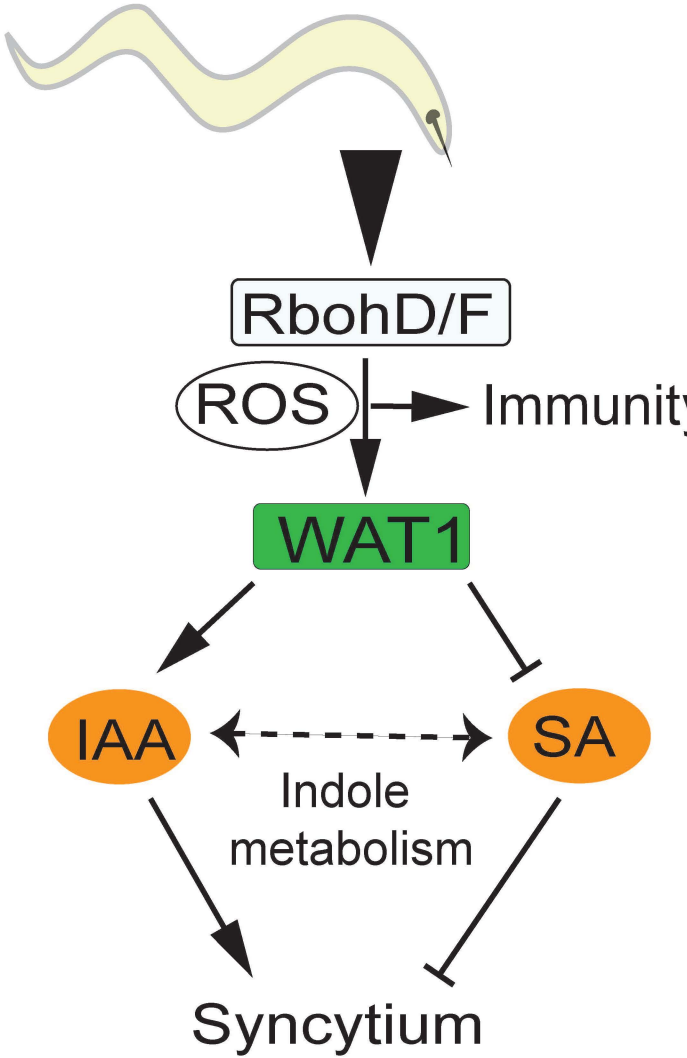
RbohD/F
ROS
Immunity
WAT1
IAA
SA
Indole
metabolism
Syncytium